RESEARCH ARTICLE

THE EFFECT OF TOPOGRAPHY ON BUILDING STRUCTURES IN URBAN SUBDIVISION UTILIZING COMPUTATIONAL FLUID DYNAMICS FOR CRITICAL WIND PRESSURE DETERMINATION

*Bonifacio Jr Aznar

Philippine Institute of Civil Engineers, Philippines

ABSTRACT

The topography was established using Autodesk Revit with reference to Google Earth. The mathematical model was formulated with the discretization of the Navier-Stokes equation in three dimensional form into a simplified and corrected momentum and pressure equations. The maximum positive and negative wind pressures were obtained from 180° south wind attack angle and critical wind pressures were obtained from the maximum negative wind pressures. Topography in terms of elevation showed that the recorded wind pressure of elevated houses are higher than those situated on the non-elevated areas. As the velocity profile and elevation of the topography increases, the simulated pressure also increases. The higher the simulation resolution, the more detailed and accurate are the results.

INTRODUCTION

Wind is one of the important forces of nature that must be considered in any structural design. Its actual behavior is influenced not only by the surface conditions, but also by the geometry of a structure. All types of turbulent effects occur, especially at corners, edges and roof eaves of a structure. Some of these effects are accounted for by the wind pressure coefficients (Cui, 2007). Wind flow generation has different types of forms, examples of these are gales and monosonic winds, cyclones/hurricanes/typhoons, tornados, thunderstorms and localized storms depending on the location and the importance of the structures being designed (Bhandari, Krishna and Kumar, 2011). Hurricane winds destroy buildings and structures around the world such as residential, commercial and industrial buildings. Boudreau (2009) mentioned that majority of the growing population in the United States lived in open terrains and coastal areas. Based on his findings, there is therefore an increasing need to conduct future researches pertaining to hurricanes. Typhoon Haiyan, otherwise known as Super Typhoon Yolanda in the Philippines, was the strongest storm recorded at landfall with a maximum sustained wind of 315 kph. With this extremely high wind speed, Typhoon Haiyan was reported to have claimed the lives of at least 6300 people and an estimated damage of $219.5 million to infrastructure alone (National Disaster Risk Reduction and Management Council [NDRRMC], 2014). In Mindanao which is located at the southern part of the Philippines, past and current practices consider dead load and live load only in the design of structures, particularly in roofing. The National Structural Code of the Philippines (NSCP) requires wind load analysis to be considered in the structural design of roofs. This is done in order to prevent further destruction caused by super typhoons, that even exceed the maximum allowable wind velocity as provided in the NSCP 2010 edition. Detailed codes and specifications are necessary in determining the minimum design requirements. However, these provisions are limited to general conditions. Projects that go beyond the basic parameters of these standards require wind tunnel testing or wind simulation. To save on cost and time, wind pressures and wind loads can be determined with the use of computer-aided simulation softwares, such as: SolidWorks, Robot Structural Analysis and Computational Fluid Dynamics (CFD) (Gallant, 2014). However, the main focus of this study is the CFD Flow Design simulation software. Computational Fluid Dynamics (CFD) has become a very useful tool in analyzing wind flows instantly. It is able to solve mathematical models accurately for any type of structure. Moreover, it is able to analyze results which can be used for design optimization (Kerklaan, 2006).

These results would lead to a more efficient structural design. Reiter (2008) states that CFD simulation programs have a huge advantage over wind tunnel tests. Through the use of CFD simulation programs, both quantitative and qualitative wind flow representation of the entire volume can be obtained. Results of these simulation programs can be used as a structural design reference. Accuracy of these tools can be proven in correlation with the following: field test results, current NSCP wind specifications and theoretical concepts. In this study, the CFD Flow Design 2014 virtual wind simulation program and Autodesk Revit Building Information Modeling 2015 were utilized in order to simulate the different wind velocities affecting the topography of a sample urban subdivision. They were also used to determine the critical wind pressures of the building structures as reference for structural design. This study is unique compared to other studies since the software used in mathematical modeling and wind simulation was new in the locality. The purpose of this study is to determine the effect of topography on building structures in urban subdivision utilizing computational fluid dynamics for critical wind pressure determination. Specifically, it has the following objectives:

- To establish the topography of sample subdivision;
- To formulate a mathematical model as input to CFD;
- To conduct simulations for varying wind velocities affecting the topography of sample subdivision; and,
- To determine the critical wind pressures of the building structures of sample subdivision.

Review of Related Literature

Wind Engineering on Structures: Wind engineering is a field in structural engineering that has been evolving over the centuries. Over 350 years ago, Torricelli invented the barometer to measure air pressure. This invention was considered as the first step in wind engineering. Measurements of the actual wind flows to predict the forces transferred to engineered structures with the use of wind tunnels in either actual or virtual was the core in wind engineering (Boudreau, 2009). The high degree of industrialization and speedy construction were the reasons why light-weight gable roof buildings had been extensively used in low-rise commercial and industrial buildings. However, their relatively light dead load and flexibility made them most vulnerable to wind load which was considered as a significant type of load in structural design (Jing and Li, 2013). These factors led to the development of various building codes relative to wind loads across the world as a design tool for structural engineers. Accurate knowledge of wind pressure and its coefficients on the walls and roofs of structures are necessary for the design of wind-resistant structures. Holmes (1994) investigated wind pressure characteristics acting on the walls and roofs of gable-roofed houses. He took into consideration the effects of elevation, roof pitch and grouping of buildings on the external pressures. The characteristics of long low-rise structures with gable roofs on the large aspect ratio were studied by Kanda and Maruta (1993). They discovered that the large negative values of mean wind pressure and peak wind pressure were generated on the leeward surface for a 45° wind attack angle. They concluded that the main sources of large negative wind pressure values were generated on the leeward side of a structure.

Meecham, Surry and Davenport (1991) evaluated the performances of gabled roof and hip roof building models. They reported the dominance of hip roof over gabled roof. Their statement was based on the result that the peak pressure on the hip roof was reduced by about 50% compared to that of the gabled roof. Holmes (1986) conducted a study on the effects of the elevation of houses and the roof pitch. His findings revealed that elevated houses performed worse than the non-elevated ones considering the same roof pitch. The 15° roof pitch recorded all negative wind pressure coefficients, while the 20° and 30° pitch had near zero and almost zero on the windward side of the roof, respectively. Prasad, Uliate and Ahmed (2008) investigated the effects of wind loads on low-rise building models. He identified the best roof configuration and found out that suction for the flat roof was the worst among the nine models. He added that the hip roof models performed better than the gabled roof models which had a 42% recorded reduction in the peak suction.

Computational fluid dynamics on structures and environment: Computational Fluid Dynamics (CFD) is used in assessing the wind flow over buildings, mountains, urban areas, etc. It is also used in assessing the atmospheric boundary layer flow and turbulence effect. The application of CFD in wind engineering has significantly increased for the past two decades from micro to macro level (Irshad, 2012). Its analysis in wind engineering is used in predicting wind climate from human to urban scale. However, due to the urban environmental complexity, the results are not yet perfect, indicating that more improvements are still necessary (Murakami, Ooka, Mochida, Yoshida and Kim, 1999). Mathematical models of All CFD programs were based on the fluid dynamic equations for mass, momentum and energy conservation. The two common types of CFD mathematical models currently used to achieve closure are the Reynolds Averaged Navier-Stokes (RANS) and Large Eddy Simulation (LES) (Irshad, 2012). RANS model equations are used to determine the transport equations for the average air flow quantities in which all the turbulence scales are simulated. The RANS model is broken down into a series of elements called voxels. These are solved using a finite volume method approach. On the other hand, the LES model equations provide an alternative approach since it adopts a spatial filtering approach. The filtering process is a computer mathematical manipulation that eliminates eddies smaller than the filter boundary. Hence, the LES model provides a more accurate and detailed simulation than RANS method especially in terms of turbulence (Clannachan, Lim, Bicanic, Taylor and Scanlon, 2009). Computational Wind Engineering (CWE) is one of the applications of CFD in wind engineering. It is used in investigating the interaction between wind and structure. Dynamic behavior of a structure and pedestrian comfort around high-rise buildings could also be investigated. All aspects of the fluid levels were determined by CFD programs. These aspects included velocity, fluid direction, pressure and turbulence (Kerklaan, 2006). CFD modeling of airflow within plant canopies using 3D canopy was used to understand the effect of the canopy. Comparison with the

wind tunnel results was presented by Endalew et al. (2009). In their study, they found that the simulation result was congruent with the average longitudinal velocity measurements having 92% minimum accuracy. The main disadvantage was that the flow problems being solved were based on theoretical models rather than on actual flow data as compared to full-scale wind tunnel models of rooftop wind flows. Araujo, de Alencar Valenca, Asibor and Rosas (2012) simulated wind flow fields around an urban environment. The objective of this simulation was to evaluate the significant impact of buildings on the wind flow patterns and power production for the current generation of wind turbines or wind mills. The roughness, topography and volumetry of buildings were considered in the simulation of the urban environment. Results showed that the simulation identified zones for potential wind sources which were not detected in classical wind atlas. Wakes, Maegli, Dickinson and Hilton (2009) studied the numerical modeling of wind flow over a complex topography for land planning purposes. This research established the numerical simulation techniques which can be used for predictive purposes. Mohotti, Mendis and Ngo (2014) studied the application of CFD in predicting the wind loads on tall buildings.

They stated that the rapid growth of CFD programs over the last few decades enabled engineers and designers to simulate wind behavior and predict wind loads on buildings, and becomes necessary especially at the preliminary design stage. CFD application for the analysis of complex urban environments was greatly improved with the increased Central Processing Unit power or memory. An accurate CFD simulation is dependent on the quality and complexity of the computational grid or mesh. A Geographic Information System (GIS) data of an urban environment can be transferred to this computational grid and utilized for simulation (Labovsky and Jelemensky, 2013). Ahmad, Muzzammil and Zaheer (2011) conducted numerical simulation of wind loads on low buildings. The simulation of the environment involved the full-scale Reynolds number, boundary layer and turbulence properties. He compared the wind loading effect of the flat roof and pitched roof using both wind simulation and wind tunnel test. Results showed that there is a fair agreement between the wind simulation and wind tunnel test on buildings. It also showed that the numerical simulation of wind loads hold a great potential in extending codes for wind loads.

Montazeri and Blocken (2013) studied on the CFD simulation of wind-induced pressure coefficients on buildings with and without balconies. Their study presented a systematic evaluation of 3D steady Reynolds Averaged Navier Stokes (RANS) CFD. It was conducted in order to predict the wind pressure distributions on the windward and leeward surfaces of a medium-rise building with and without balconies. Findings revealed that RANS, can accurately reproduce the wind pressure distribution across the windward face of the building with the average deviations from the wind tunnel measurements of 12% and 10% for the building with and without balconies, respectively. Computational evaluation of wind loads on buildings were studied by Dagnew and Bitsuamlak (2012). They reviewed the CFD numerical evaluation of wind loads on buildings. They also reported the advantages of LES over RANS and hybrid RANS-LES over LES. They added that LES based simulations seem suitable for wind load evaluation and that the numerical and experimental wind load evaluation on buildings were in good agreements on the mean values. Wind tunnel simulations were employed by Lee, Park and Kang (2009). They utilized these simulations in evaluating the wind environment around a tested residential area located near industrial complexes.

They reported that in the upper region, the velocity fluctuations increased and in the near surface layer the wind speed decreased due to the presence of hills and high rise structures around the simulated area. Hang, Sandberg and Li (2009) studied the effect of urban morphology on wind condition in idealized city models. These includes round, square and long rectangular city model with a developed steady flow region along the main street. They also found that a weaker wind was observed in the street of the square city model than that observed in the round city model. Meanwhile, a steady horizontal flow along the street with an approximate fully developed region was observed in the long rectangular city model. Computational Wind Engineering (CWE) over the years had grown to a strongly established field in wind engineering practice, education and research. It was used daily by thousands of practitioners, instructors and researchers around the world (Assaad, 2015). CFD Flow Design is widely recognized as a simple CFD, due to its less setup options and interoperability with other autodesk softwares, such as: revit and autocad 3ds max. It is also commonly used in analyzing external wind pressure that serves as a good reference in calculating external wind loads for structural design purposes (Autodeskcfd-fd, 2015). Broekhuizen (2016) compared the 2D and 3D simulation using CFD Flow Design. He observed that 3D simulation provided a more accurate result compared to 2D simulation due to its environmental complexity. He also found out that the quality of the simulation could be set from 50% to 400%, wherein higher resolution means a more detailed and accurate but slower simulation. Autodeskcfd-fd (2015) reported that the quality of the simulation depended on the simulation resolution. The lower the resolution the faster but less detailed and less accurate was the simulation. On the other hand, the higher the resolution the slower but the more detailed and more accurate was the simulation. Autodeskcfd-fd (2015) also added that the simulation resolution was dependent upon the Random Access Memory (RAM) resources of a computer. The higher the RAM the higher was the simulation resolution. This study is aimed to use the Computational Fluid Dynamics (CFD) Flow Design virtual wind simulation. This will be used for the mathematical and building models subjected to different wind velocities affecting the topography of a sample subdivision. It also aimed to determine the critical wind pressure of the structures as reference/basis for structural design, particularly in roofing.

Significance of the study: Through this study, engineers and designers would be able to use a wind simulation software that considered all wind load effects, most especially, topography. This would be applicable to any type of structure. Moreover, it would minimize the time and cost involved in the project. The output of this study can be used by a structural engineer as parameter in designing building structures located at Cabantian, Davao city. The result of this study can also be used as reference for future researches involving wind simulation in other places in Mindanao along the coastal areas especially in the Pacific Ocean.

METHODS

Research Design: This research is a modeling and simulation study. A simulation study involves the following key stages namely: conceptual model, computer model, solutions/understanding and Improvement in the real world. A conceptual model is a model description which is to be developed in a computer software. A computer model is the simulation model enforced which in this case is the wind simulation software. Solutions/understanding is derived from the results of the experiment. Lastly, improvement in the real world is acquired from implementing the solutions formed (Robinson, 2004). Prior to this study, the topography of sample subdivision, mathematical model and velocity profiles as input to simulation and critical wind pressures of the structures should be established. The simulation process took a total of 60 hours with 12 hours per wind velocity profile simulation in order to arrive at the most accurate results. The results are then presented in tables and figures.

Research Locale: The research locale of the urban subdivision was at Deca Homes Cabantian, Davao City, Philippines. The maps were based from Google map and Google Earth Pro. These maps were utilized as input data for the simulation.

Data Collection: The data collection for each specific objective were explained thoroughly in the paragraphs below.

Topography of sample subdivision: A Computer-Aided Design (CAD) model with reference to Google Earth Pro was used in order to come-up with the topography of Deca Homes Cabantian, Davao City.

Mathematical model as input to CFD: The sample building models together with the distances between the buildings and their surroundings were also derived using Computer-Aided Design (CAD). The mathematical model of the Computational Fluid Dynamics (CFD) Flow Design was based on the Fluid Dynamic equation: Reynolds Averaged Navier-Stokes (RANS) and Large Eddy Simulation (LES), which accounted for the turbulence model just like a traditional CFD application (Clannachan *et al.,* 2009). After a thorough study, the fluid dynamic equation was improved to the low Mach number assumption to decompose the pressure. Mach One (1) is equal to the speed of sound (343.2m/s).

Mach numbers less than 0.3 (103m/s) are assumed to have incompressible flows whereas Mach numbers greater than 0.3 requires the consideration of compressible analysis for accurate solutions (Autodeskcfd, 2016). Incompressible flows uses a pressure correction equation based on the work of Patankar and Spalding (1972). These researchers developed the initial implementation of the SIMPLE (Semi Implicit Method for Pressure Linked Equations) algorithm. The SIMPLE algorithm method starts with the initial pressure values P^n derived from the simulation. The researcher then determined the mass flow rate at the element faces using the Rhie-Chow interpolation to compute a momentum satisfying mass flow rate field $_m{}^*$. Using the new mass flow rates, the pressure correction equation was assembled and solved to obtain a pressure correction field P'. Finally, the researcher obtained the collocated pressure correction using the equation: $Pc^* = Pc^n + Pc'$ where Pc^* is the collocated pressure correction, Pc^n is the simulated initial guess for pressure cell or center and Pc' is the pressure correction (Moukalled *et al.,* 2016).

Varying wind velocities affecting the topography of sample subdivision: The velocity profiles entered and applied were adapted from the American Society of Civil Engineers (ASCE) / National Structural Code of the Philippines (NSCP) wind specifications, such as: 150kph (41.67m/s), 200kph (55.56m/s) and 250kph (69.44m/s), respectively. Furthermore, wind speeds of 300kph (83.33m/s) and 350kph (97.22m/s) were added by the researcher to consider the velocity of super typhoons like Pablo and Yolanda.

Critical wind pressures of the building structures of sample subdivision: The maximum positive and negative wind pressures of the building structures were generated by the Autodesk Computational Fluid Dynamics (CFD) Flow Design simulation software. The critical wind pressures were also obtained using CFD Flow Design.

Research Tools: The research tools used in the study were the Autodesk Revit Building Information Modeling 2015 and the Autodesk Computational Fluid Dynamics (CFD) Flow Design 2014 Simulation software. These programs were utilized since it has both the topographic-building modeling and wind simulation capabilities. Moreover, these softwares are user friendly due to their convenient user interface compared with other simulation programs.

RESULTS

Topography of Sample Subdivision: In this study a Computer-Aided Design (CAD) model of the topography of Deca Homes, Cabantian, Davao City was made with reference to Google Earth Pro. The approximate area of the sample subdivision is 11.5 hectares or 115000 square meters (m^2). In the south view of the topography, the maximum elevation on the right side is 8 meters followed by intervals of 6 meters, 4 meters and 2 meters, respectively. On the left side, the maximum elevation is 8 meters followed by intervals of 6.4 meters, 4.8 meters, 3.2 meters and 1.6 meters, respectively. Contour intervals of 40 meters was applied on each respective elevation intervals.

The datum/reference at elevation 0 meter was taken at the 25 meter part of the topography as shown in Figure 1.
Figure 1 shows the area of topography and contour intervals of sample urban subdivision. The approximate area of topography of the sample urban subdivision is 11.5 hectares. Contour intervals of 40 meters was applied on each respective elevation intervals on

the east (right) and west(left) sides of the topography. The datum/reference elevation at 0 meter was taken at the 25 meter part of the topography were the drainage and the two main parallel roads of the subdivision was located.
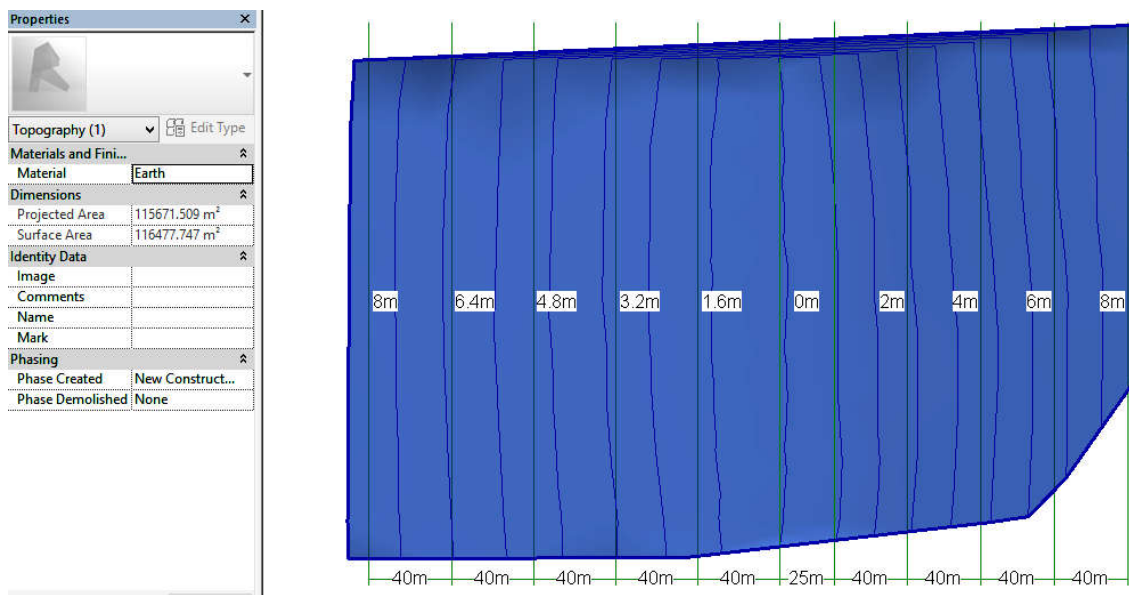

Figure 1. Area of Topography and Contour Intervals of Sample Urban Subdivision

Mathematical Model as Input to CFD: The mathematical model as input to CFD was derived from the Navier Stokes equation in three dimensional Cartesian coordinates followed by the discretization with respect to volume and surface integration and then by numerical methods using finite volume method for the pressure correction equation.

The Navier Stokes equation in three dimensional Cartesian coordinates is given by

$$\rho\frac{\partial u}{\partial t} + \rho u\frac{\partial u}{\partial x} + \rho v\frac{\partial u}{\partial y} + \rho w\frac{\partial u}{\partial z} = -\frac{\partial P}{\partial x} + \mu\left[\frac{\partial^2 u}{\partial x^2} + \frac{\partial^2 u}{\partial y^2} + \frac{\partial^2 u}{\partial z^2}\right] \tag{3.1}$$

$$\rho\frac{\partial v}{\partial t} + \rho u\frac{\partial v}{\partial x} + \rho v\frac{\partial v}{\partial y} + \rho w\frac{\partial v}{\partial z} = -\frac{\partial P}{\partial y} + \mu\left[\frac{\partial^2 v}{\partial x^2} + \frac{\partial^2 v}{\partial y^2} + \frac{\partial^2 v}{\partial z^2}\right] \tag{3.2}$$

$$\rho\frac{\partial w}{\partial t} + \rho u\frac{\partial w}{\partial x} + \rho v\frac{\partial w}{\partial y} + \rho w\frac{\partial w}{\partial z} = -\frac{\partial P}{\partial z} + \mu\left[\frac{\partial^2 w}{\partial x^2} + \frac{\partial^2 w}{\partial y^2} + \frac{\partial^2 w}{\partial z^2}\right] \tag{3.3}$$

where:

$$\rho\frac{\partial u}{\partial t}, \rho\frac{\partial v}{\partial t}, \rho\frac{\partial w}{\partial t}$$ are the local acceleration along x, y and z axes, respectively

$$\rho u\frac{\partial u}{\partial x} + \rho v\frac{\partial u}{\partial y} + \rho w\frac{\partial u}{\partial z}, \rho u\frac{\partial v}{\partial x} + \rho v\frac{\partial v}{\partial y} + \rho w\frac{\partial v}{\partial z}, \rho u\frac{\partial w}{\partial x} + \rho v\frac{\partial w}{\partial y} + \rho w\frac{\partial w}{\partial z}$$

are the convection along x, y and z axes, respectively

$$-\frac{\partial P}{\partial x}, -\frac{\partial P}{\partial y}, -\frac{\partial P}{\partial z}$$

are the piezometric pressure gradient along x, y and z axes, respectively

$$\mu\left[\frac{\partial^2 u}{\partial x^2} + \frac{\partial^2 u}{\partial y^2} + \frac{\partial^2 u}{\partial z^2}\right], \mu\left[\frac{\partial^2 v}{\partial x^2} + \frac{\partial^2 v}{\partial y^2} + \frac{\partial^2 v}{\partial z^2}\right], \mu\left[\frac{\partial^2 w}{\partial x^2} + \frac{\partial^2 w}{\partial y^2} + \frac{\partial^2 w}{\partial z^2}\right]$$

are the viscous terms along x, y and z axes, respectively

The Continuity equation in three dimensional Cartesian coordinates is given by

$$\frac{\partial \rho}{\partial t} + \frac{\partial (\rho u)}{\partial x} + \frac{\partial (\rho v)}{\partial y} + \frac{\partial (\rho w)}{\partial z} = 0$$

(3.4)

or

$$\frac{\partial \rho}{\partial t} + \nabla \bullet (\rho v) = 0$$

(3.5)

where in Cartesian coordinates, the vector operator nabla (del), ∇, is defined as

$$\nabla = \frac{\partial}{\partial x} i + \frac{\partial}{\partial y} j + \frac{\partial}{\partial z} k$$

The continuity equation is a partial differential equation form of the continuity condition. This represents an unsteady, three-dimensional mass conservation at a point in a compressible fluid. This infinitesimally small aspect of the element is why the equation is directly obtained in this form. Solving general flows requires an algorithm that can deal with the pressure-velocity coupling. The classical segregated SIMPLE (Semi Implicit Method for Pressure Linked Equations) algorithm of Patankar and Spalding (1972) was used to iteratively solve the Navier-Stokes equations. The Navier-Stokes equations was reformulated in terms of a momentum and a pressure equation, which are then discretized and solved sequentially. The pressure equation is constructed by combining the semi-discretized momentum and continuity equations.

For steady and incompressible flows, the simplified continuity and momentum equations becomes

$$\frac{\partial (\rho u)}{\partial x} + \frac{\partial (\rho v)}{\partial y} + \frac{\partial (\rho w)}{\partial z} = 0$$

(3.6)

$$\frac{\partial (\rho uu)}{\partial x} + \frac{\partial (\rho vv)}{\partial y} + \frac{\partial (\rho ww)}{\partial z} = \frac{\partial}{\partial x}\left(\mu \frac{\partial u}{\partial x} \right) + \frac{\partial}{\partial y}\left(\mu \frac{\partial v}{\partial y} \right) + \frac{\partial}{\partial z}\left(\mu \frac{\partial w}{\partial z} \right) - \frac{\partial P}{\partial x} - \frac{\partial P}{\partial y} - \frac{\partial P}{\partial z}$$

(3.7)

Figure 2 shows the top and side views of a building taken from the sample subdivision and is used to derive the pressure correction equation for the three dimensional Cartesian grid.
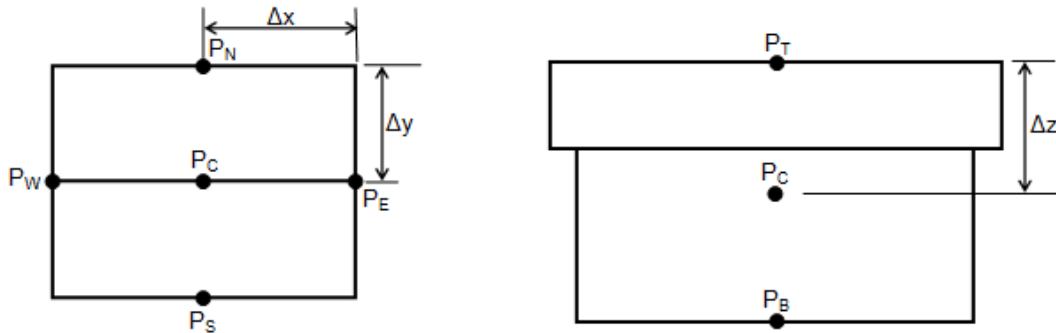

Figure 2. Top and Side View of a Structure

The discretization of momentum equation starts with volume integration and is shown as

$$\int_{Vc}\frac{\partial (\rho uu)}{\partial x}dV + \int_{Vc}\frac{\partial (\rho vv)}{\partial y}dV \int_{Vc}\frac{\partial (\rho ww)}{\partial z}dV = \int_{Vc}\frac{\partial}{\partial x}\left(\mu \frac{\partial u}{\partial x} \right)dV + \int_{Vc}\frac{\partial}{\partial y}\left(\mu \frac{\partial v}{\partial y} \right)dV$$

$$+ \int_{Vc}\frac{\partial}{\partial z}\left(\mu \frac{\partial w}{\partial z} \right)dV - \int_{Vc}\frac{\partial P}{\partial x}dV - \int_{Vc}\frac{\partial P}{\partial y}dV - \int_{Vc}\frac{\partial P}{\partial z}dV$$

(3.8)

Volume integrals of the convection and diffusion terms are then transformed into surface integrals by invoking the divergence theorem to give

$$\int_{\partial Vc} (\rho uu) dydz + \int_{\partial Vc} (\rho vv) dxdz + \int_{\partial Vc} (\rho ww) dxdy = \int_{\partial Vc} \left(\mu \frac{\partial u}{\partial x} \right) dydz + \int_{\partial Vc} \left(\mu \frac{\partial v}{\partial y} \right) dxdz$$

$$+ \int_{\partial Vc} \left(\mu \frac{\partial w}{\partial z} \right) dxdy - \int_{Vc} \frac{\partial P}{\partial x} dV - \int_{Vc} \frac{\partial P}{\partial y} dV - \int_{Vc} \frac{\partial P}{\partial z} dV$$

$$(3.9)$$

Representing the surface integrals by summation of fluxes over the faces of the element, and using a single Gaussian point for the face integrals, the semi-discretized forms of the three dimensional sides of Equation 3.9 becomes

$$\left(\rho u \Delta y \Delta z \right)_e u_e - \left(\rho u \Delta y \Delta z \right)_w u_w + \left(\rho v \Delta x \Delta z \right)_n u_n - \left(\rho v \Delta x \Delta z \right)_s u_s + \left(\rho w \Delta x \Delta y \right)_t u_t$$

$$- \left(\rho w \Delta x \Delta y \right)_b u_b = \left(\mu \frac{\partial u}{\partial x} \Delta y \Delta z \right)_e + \left(\mu \frac{\partial v}{\partial y} \Delta x \Delta z \right)_n + \left(\mu \frac{\partial w}{\partial z} \Delta x \Delta y \right)_t - \left(\mu \frac{\partial u}{\partial x} \Delta y \Delta z \right)_w$$

$$- \left(\mu \frac{\partial v}{\partial y} \Delta x \Delta z \right)_s - \left(\mu \frac{\partial w}{\partial z} \Delta x \Delta y \right)_b - \int \frac{\partial P}{\partial x} dV - \int \frac{\partial P}{\partial y} dV - \int \frac{\partial P}{\partial z} dV$$

$$(3.10)$$

Equation (3.10) can be simplified as

$$\dot{m}_e u_e + \dot{m}_w u_w + \dot{m}_n u_n + \dot{m}_s u_s + \dot{m}_t u_t + \dot{m}_b u_b - \left[\left(\mu \frac{\partial u}{\partial x} \Delta y \Delta z \right)_e - \left(\mu \frac{\partial u}{\partial x} \Delta y \Delta z \right)_w \right]$$

$$- \left[\left(\mu \frac{\partial v}{\partial y} \Delta x \Delta z \right)_n - \left(\mu \frac{\partial v}{\partial y} \Delta x \Delta z \right)_s \right] - \left[\left(\mu \frac{\partial w}{\partial z} \Delta x \Delta y \right)_t - \left(\mu \frac{\partial w}{\partial z} \Delta x \Delta y \right)_b \right] = -\int \frac{\partial P}{\partial x} dV$$

$$- \int \frac{\partial P}{\partial y} dV - \int \frac{\partial P}{\partial z} dV$$

$$(3.11)$$

The discretization of the continuity equation starts from the simplified continuity equation and integrating over element C to give

$$\int_{Vc} \frac{\partial (\rho u)}{\partial x} dV + \int_{Vc} \frac{\partial (\rho v)}{\partial y} dV + \int_{Vc} \frac{\partial (\rho w)}{\partial z} dV = 0$$

$$(3.12)$$

Using the divergence theorem to transform to give volume integral into a surface integral and then into summation of fluxes over the faces of the element, the discrete form of the continuity equation is obtained as

$$(\rho u \Delta y \Delta z)_e - (\rho u \Delta y \Delta z)_w + (\rho v \Delta x \Delta z)_n - (\rho v \Delta x \Delta z)_s + (\rho w \Delta x \Delta y)_t - (\rho w \Delta x \Delta y)_b = 0$$

$$(3.13)$$

or

$$\dot{m}_e + \dot{m}_w + \dot{m}_n + \dot{m}_s + \dot{m}_t + \dot{m}_b = 0$$

$$(3.14)$$

The discretization of the pressure term can be accomplished by transforming the pressure gradient term of the volume integral into a surface integral as shown as

$$\int_{Vc} \frac{\partial P}{\partial x} dV + \int_{Vc} \frac{\partial P}{\partial y} dV + \int_{Vc} \frac{\partial P}{\partial z} dV = \int_{\partial Vc} P dydz + \int_{\partial Vc} P dxdz + \int_{\partial Vc} P dxdy$$

$$\int_{Vc}\frac{\partial P}{\partial x}dV + \int_{Vc}\frac{\partial P}{\partial y}dV + \int_{Vc}\frac{\partial P}{\partial z}dV = (P\Delta y\Delta z)_e - (P\Delta y\Delta z)_w + (P\Delta x\Delta z)_n - (P\Delta x\Delta z)_s$$
$$+ (P\Delta x\Delta y)_t - (P\Delta x\Delta y)_b$$
$$\int_{Vc}\frac{\partial P}{\partial x}dV + \int_{Vc}\frac{\partial P}{\partial y}dV + \int_{Vc}\frac{\partial P}{\partial z}dV = (P_e - P_w)\Delta y\Delta z + (P_n - P_s)\Delta x\Delta z + (P_t - P_b)\Delta x\Delta y$$
$$\int_{Vc}\frac{\partial P}{\partial x}dV + \int_{Vc}\frac{\partial P}{\partial y}dV + \int_{Vc}\frac{\partial P}{\partial z}dV = (P_e - P_w)\frac{Vc}{\Delta x} + (P_n - P_s)\frac{Vc}{\Delta y} + (P_t - P_b)\frac{Vc}{\Delta z}$$

(3.15)

Applying linear interpolation profile for the variation of pressure as shown gives

$$\int_{Vc}\frac{\partial P}{\partial x}dV + \int_{Vc}\frac{\partial P}{\partial y}dV + \int_{Vc}\frac{\partial P}{\partial z}dV = \left[\frac{1}{2}(P_e + P_c) - \frac{1}{2}(P_c + P_w)\right]\frac{Vc}{\Delta x} + \left[\frac{1}{2}(P_n + P_c) - \frac{1}{2}(P_c + P_s)\right]\frac{Vc}{\Delta y}$$
$$+ \left[\frac{1}{2}(P_t + P_c) - \frac{1}{2}(P_c + P_b)\right]\frac{Vc}{\Delta z}$$
$$\int_{Vc}\frac{\partial P}{\partial x}dV + \int_{Vc}\frac{\partial P}{\partial y}dV + \int_{Vc}\frac{\partial P}{\partial z}dV = \frac{(P_e - P_w)Vc}{2\Delta x} + \frac{(P_n - P_s)Vc}{2\Delta y} + \frac{(P_t - P_b)Vc}{2\Delta z}$$
$$\int_{Vc}\frac{\partial P}{\partial x}dV + \int_{Vc}\frac{\partial P}{\partial y}dV + \int_{Vc}\frac{\partial P}{\partial z}dV = \frac{Vc}{2}\left[\frac{P_e - P_w}{\Delta x} + \frac{P_n - P_s}{\Delta y} + \frac{P_t - P_b}{\Delta z}\right]$$

(3.16)

The Pressure Correction Equation The derivations are based on the work of Patankar and Spalding (1972), who developed the initial implementation of the SIMPLE (Semi Implicit Method for Pressure Linked Equations) algorithm. The SIMPLE algorithm starts with the continuity and momentum equations as derived earlier and then proceeds by providing initial guess for the velocity and pressure fields.

The pressure correction equation is given by

$$P^* = P^n + P'$$

(3.17)

where P* is the collocated pressure correction, Pn is the simulated initial guess for pressure cell and P' is the pressure correction. The mass flow rate at cell faces correction is given by

$$(\dot m_e{}^* + \dot m_e') + (\dot m_w{}^* + \dot m_w') + (\dot m_n{}^* + \dot m_n') + (\dot m_s{}^* + \dot m_s') + (\dot m_t{}^* + \dot m_t') + (\dot m_b{}^* + \dot m_b') = 0$$

$$\dot m_e' + \dot m_w' + \dot m_n' + \dot m_s' + \dot m_t' + \dot m_b' = -\dot m_e{}^* - \dot m_w{}^* - \dot m_n{}^* - \dot m_s{}^* - \dot m_t{}^* - \dot m_b{}^*$$

(3.18)

where the mass flow rates and mass flow rate corrections at an element faces are

$$\dot m_e = (\rho u\Delta y\Delta z)_e, \dot m_w = -(\rho u\Delta y\Delta z)_w, \dot m_n = (\rho v\Delta x\Delta z)_n, \dot m_s = -(\rho v\Delta x\Delta z)_s,$$

$$\dot m_t = (\rho w\Delta x\Delta y)_t, \dot m_b = -(\rho w\Delta x\Delta y)_b$$

and

$$\dot m_e' = (\rho u'\Delta y\Delta z)_e, \dot m_w' = -(\rho u'\Delta y\Delta z)_w, \dot m_n' = (\rho v'\Delta x\Delta z)_n, \dot m_s' = -(\rho v'\Delta x\Delta z)_s,$$

$$\dot m_t' = (\rho w'\Delta x\Delta y)_t, \dot m_b' = -(\rho w'\Delta x\Delta y)_b$$

so that the simplified form of equation 3.18 can be written as

$$-(\dot m_e{}^* + \dot m_w{}^* + \dot m_n{}^* + \dot m_s{}^* + \dot m_t{}^* + \dot m_b{}^*) = (\rho u'\Delta y\Delta z)_e - (\rho u'\Delta y\Delta z)_w$$
$$+ (\rho v'\Delta x\Delta z)_n - (\rho v'\Delta x\Delta z)_s + (\rho w'\Delta x\Delta y)_t - (\rho w'\Delta x\Delta y)_b$$

(3.19)

The pressure correction equation in three dimensional grid taken from the top and side views of the three dimensional domain as shown in Figure 2, where the u, v and w velocity components are stored at the (e,w), (n,s) and (t,b) element faces, is given by

$$a_C^{P'} P'_C + a_E^{P'} P'_E + a_W^{P'} P'_W + a_N^{P'} P'_N + a_S^{P'} P'_S + a_T^{P'} P'_T + a_B^{P'} P'_B = b_C^{P'} \qquad (3.20)$$

where

$$a_E^{P'} = -(\rho D^u \Delta y \Delta z)_e, a_W^{P'} = -(\rho D^u \Delta y \Delta z)_w, a_N^{P'} = -(\rho D^v \Delta x \Delta z)_n, a_S^{P'} = -(\rho D^v \Delta x \Delta z)_s,$$

$$a_T^{P'} = -(\rho D^w \Delta x \Delta y)_t, a_B^{P'} = -(\rho D^w \Delta x \Delta y)_b$$

$$a_C^{P'} = -(a_E^{P'} + a_W^{P'} + a_N^{P'} + a_S^{P'} + a_T^{P'} + a_B^{P'})$$

$$b_C^{P'} = -(\dot{m}_e^* + \dot{m}_w^* + \dot{m}_n^* + \dot{m}_s^* + \dot{m}_t^* + \dot{m}_b^*)$$

The sample building structures which are made up of gabled roofs with dimensions of 8 meters as the width, 10 meters as the length and 3 meters as the height were subjected to a roof angle of 20°. The mathematical model equation of the Autodesk Computational Fluid Dynamics (CFD) Flow Design uses the low Mach number assumption to decompose the pressure. Incompressible flows are assumed for all simulated velocity profiles since the Mach numbers for each velocity profile were found out to be less than 0.3 (103m/s) as shown in Table 1.

CFD Flow Design simulation model was based on the Reynolds Averaged Navier-Stokes (RANS) and Large Eddy Simulation (LES) which accounted for the turbulence model as shown in Figure 4.

Table 1 shows the simulated velocity profiles and their equivalent Mach numbers. Since the equivalent Mach numbers of all velocity profiles are less than 0.3, the air flow is assumed to be incompressible. Wind velocities with equivalent Mach numbers greater than 0.3, compressible effects are becoming more influential and must be considered for accurate solutions.

Table 1. Velocity Profiles with their Equivalent Mach Numbers

Velocity		Mach number
(kph)	(m/s)	$Mn_i = \dfrac{0.3 V_{(m/s)}}{103_{(m/s)}}$
150	41.67	0.121
200	55.56	0.162
250	69.44	0.202
300	83.33	0.243
350	97.22	0.283

Critical Wind Pressures of the Building Structures of Sample Subdivision: The maximum positive and negative wind pressures (0.827,-1.222; 1.662,-2.293; 2.539,-3.558; 4.099,-5.087; 5.132,-6.766) kPa were obtained from 180° south wind attack angle and their respective velocities as shown in Table 2. The sign convention of the wind pressure indicates the direction of wind on the surface of the building model: positive value indicates the wind pressure acting towards the surface and negative value indicates the wind pressure acting away from the surface. The respective critical wind pressures, wind direction and wind velocities are shown in Figures 3 to 4. Wind pressures at different wind velocities are shown in Table 2. The Simulated and theoretical absolute maximum wind pressure results are shown in Table 3. Table 2 shows the simulated results of wind pressures subjected to different wind velocities. Pressure points were shown to provide information regarding the positive (windward) and negative (leeward) wind pressures affecting the surface of the building models. The maximum negative wind pressures were evidently higher than the maximum positive wind pressures. At various wind velocities, maximum positive and negative wind pressures occur at pressure points 1 and 7.

Table 2. Wind Pressures at Different Wind Velocities

Wind Velocity (kph)	Pressure Points (kPa)						
	1	2	3	4	5	6	7
150	0.827	0.485	0.144	-0.198	-0.539	-0.881	-1.222
200	1.662	1.003	0.344	-0.315	-0.974	-1.633	-2.293
250	2.539	1.523	0.507	-0.509	-1.526	-2.542	-3.558
300	4.099	2.568	1.037	-0.494	-2.025	-3.556	-5.087
350	5.132	3.149	1.166	-0.817	-2.800	-4.783	-6.766

Table 3 shows the comparison of the absolute maximum value of the simulated and theoretical wind pressures at various wind velocities. It is shown that the simulated pressures are comparatively higher than the reference theoretical pressures since the simulated pressure varies with respect to the structure's position, location and elevation, while the theoretical pressure is taken as uniform throughout the entire sample subdivision. The simulated wind pressures were based on the pressure point 7.

Table 3. Simulated and Theoretical Wind Pressure with Respect to Wind Velocities

Velocity(V) (kph)	Simulated pressure (kPa)	Theoretical pressure $\rho = 0.0000473V^2$ (kPa)
150	1.222	1.064
200	2.293	1.892
250	3.558	2.956
300	5.087	4.257
350	6.766	5.794

Figure 3 shows the wind direction taken from south (180°) attack angle with a wind velocity of 97.22m/s (350kph) applied at the urban subdivision. The critical positive and negative wind pressures obtained were 5.132kPa and -6.766kPa, respectively. The lower wind pressures as indicated by red-orange color are mostly located at the center/lower and plain portion of the urban subdivision. The maximum positive and negative wind pressures as indicated by yellow and blue color are mostly located at the sides/upper and elevated portion of the urban subdivision especially at the south direction where the wind originates. Turbulence of the air flow was reduced when it passes through a wall boundary.
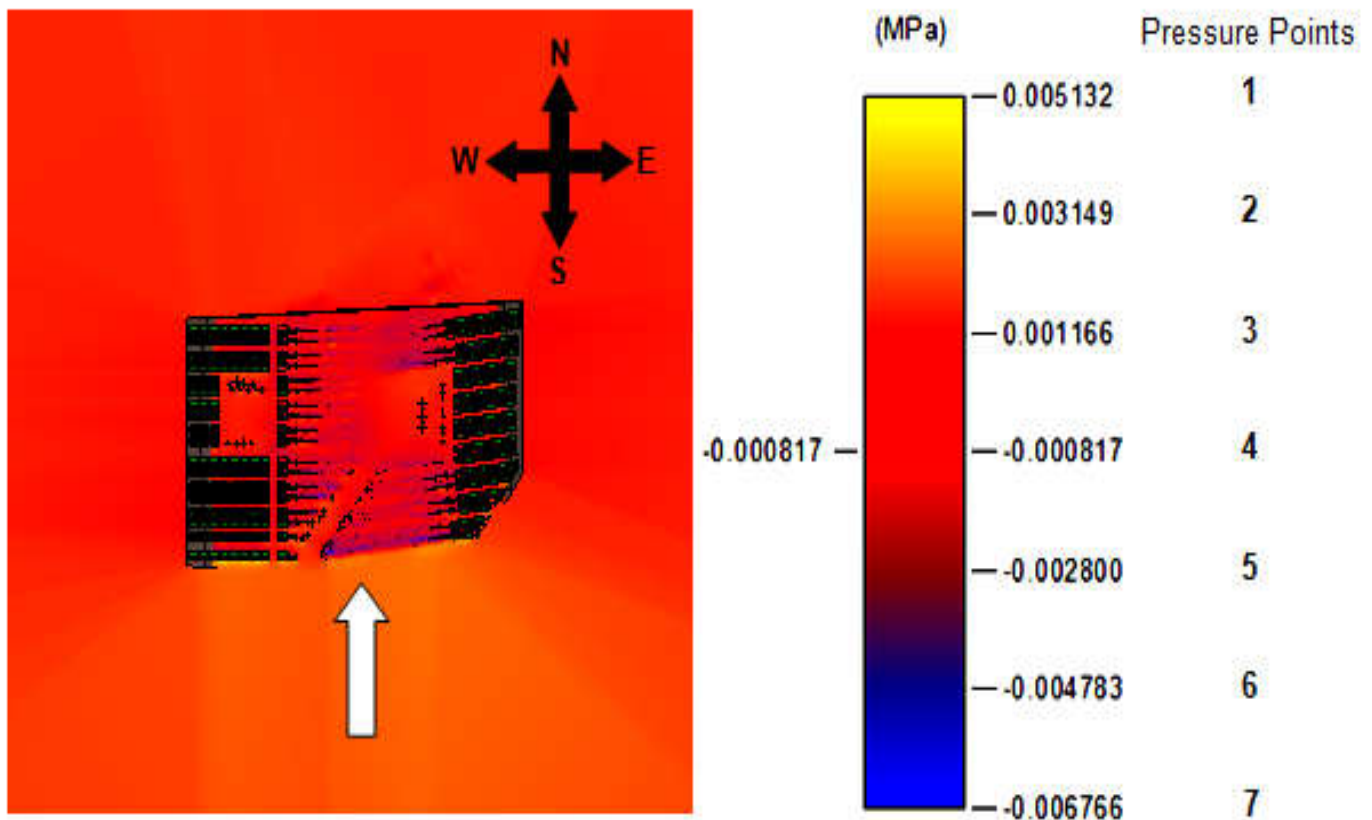

Figure 3. Wind direction from south (180°), wind velocity of 97.22m/s (350kph) and critical wind pressures

Figure 4 shows the enlarged top view with pressure points and contour intervals of simulated urban subdivision. Pressure point 1 is named as the maximum positive wind pressure and denoted as Pmax+, while pressure point 7 is named as the maximum negative wind pressure and denoted as Pmax-. These maximum wind pressures are commonly located at the upper left and right portion of the subdivision. Pressure points 2 to 7 are called as the intermediate pressure points and are commonly located at the center and lower portions of the subdivision. These intermediate pressure points are denoted as P2, P3, P4, P5 and P6, respectively.

Topography of sample subdivision: Topography in terms of elevation of the subdivision is considered in this study, the elevated houses (situated from either left side or right side of the topographic view of the urban subdivision) as shown in Figure 4 have higher recorded wind pressures compared to those which are situated on the non-elevated areas (situated at the center of the topographic view of the urban subdivision) as shown in Figure 4. The turbulence of the airflow reduced when it passes through a boundary (wall, roof, tree and the like). These findings conform with the results of Holmes (1986) on the investigation of the effects of the elevation of houses and the roof pitch. Furthermore, the results of this study also agree with the findings of Lee *et al.* (2009) which state that the velocity fluctuations in the upper region increases and the wind speed decreases in the near surface layer.
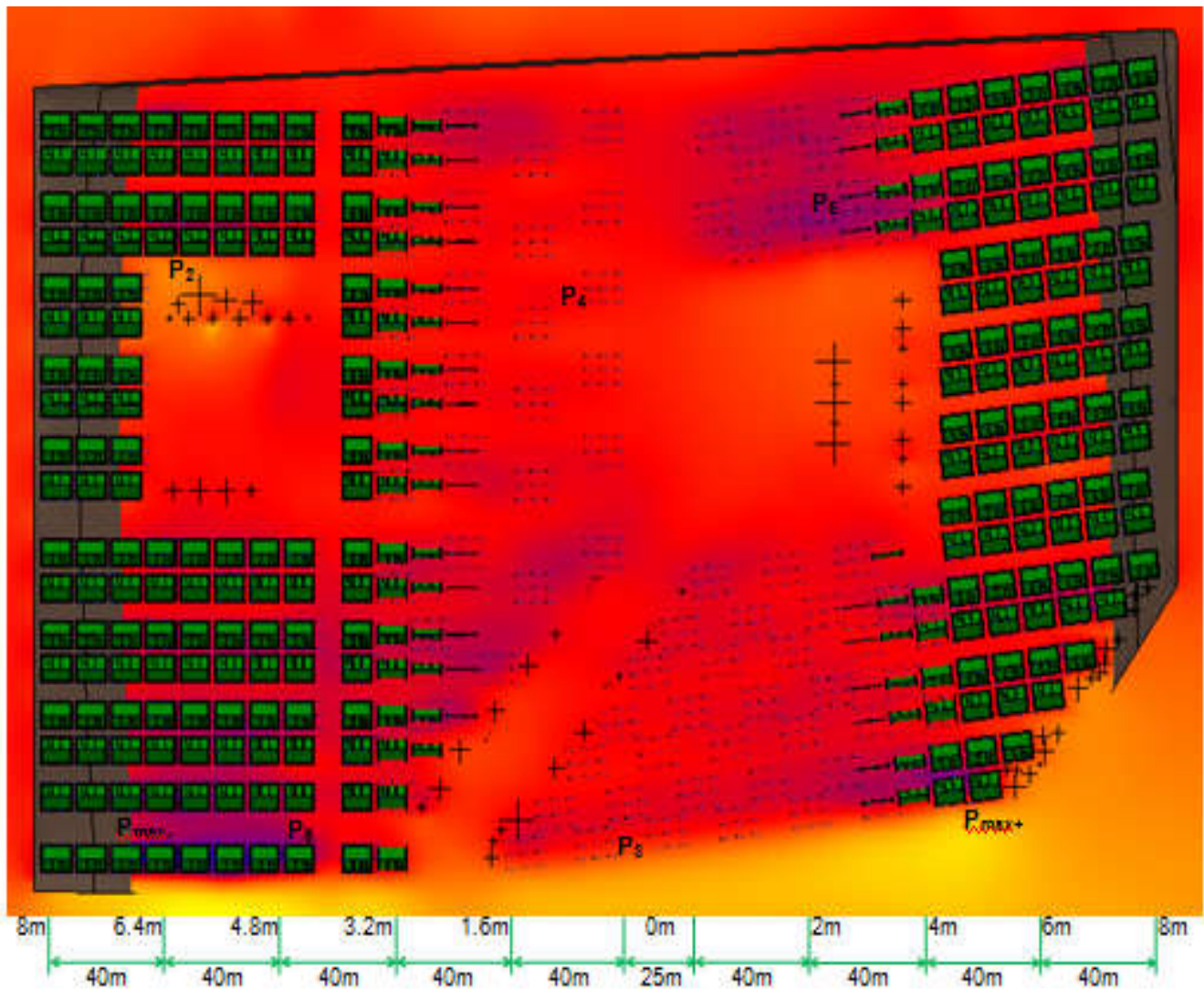
Figure 4. Enlarged Top View with Pressure Points and Contour Intervals of Simulated Urban Subdivision

Mathematical model as input to CFD

The mathematical model equation as input to Computational Fluid Dynamics (CFD) Flow Design was based on the Reynolds Averaged Navier Stokes (RANS) and Large Eddy Simulation (LES) for the turbulence model and the low Mach number assumption (Mach numbers less than 0.3 or 103m/s) to decompose the fluid dynamic equation (Boussinesq approximation) into a simpler equation. Incompressible flows for the collocated pressure and velocity correction was based on the SIMPLE (Semi Implicit Method for Pressure Linked Equations) algorithm. The SIMPLE algorithm method uses the initial pressure values derived from the wind simulation and the Rhie-Chow interpolation to solve for the pressure correction and the collocated pressure correction as shown and discussed.

These findings conforms with the study of Montazeri and Blocken (2013), who stated that RANS can accurately reproduce the wind pressure distribution especially across the windward face of the building. Gable roof buildings were used in the low-rise urban subdivision. The researcher chose this type of roofing since it is commonly used in urban subdivisions. Since gable roofs are prone to strong wind destruction, there is a need to have a complete structural analysis and design on dead, live and wind loads. This is in consonance with the study of Jing and Li (2013), who described that gable roofs are light-weight and flexible which make them most liable to wind load that is considered as a significant type of load in structural design.

Varying wind velocities affecting the topography of sample subdivision

Wind velocities of 150kph, 200kph and 250kph are standard values according to the American Society of Civil Engineers (ASCE)/National Structural Code of the Philippines (NSCP) wind load specifications. The researcher added wind velocities of 300kph and 350kph to consider the wind velocities of super typhoons. These high wind speeds are not yet included in the ASCE/NSCP, but were used by the researcher to investigate the effect of such velocities on the sample urban subdivision.

Irshad (2012) made use of Computational Fluid Dynamics (CFD) in assessing wind flow over buildings and urban areas. Kerklaan (2006) stated that CFD is used in investigating the interaction between wind and structure. He also stated that CFD programs determines all aspects of the fluid levels which includes velocity, fluid direction, pressure and turbulence. Their observation validates the use of CFD in the present study.

Critical wind pressures of the building Structures of sample subdivision

After hours of simulation, the maximum wind pressures were obtained. As the velocity profile and elevation of the topography increases, the simulated pressure also increases. As shown in Table 3, the simulated absolute maximum pressures at different velocities have values which are comparable to the theoretical pressure based on the Duchemin's formula, $\rho=0.0000473V^2$. The simulation resolution value was set to 200% to ensure a slower but a more accurate simulation. Both Autodeskcfd-fd (2015) and Broekhuizen (2016) found that the quality of simulation results is based on the simulation resolution, wherein higher resolution means a more detailed and accurate but slower simulation. Their findings support the results of this study. Autodesk CFD Flow Design provides a simple virtual wind tunnel since it is easy to setup and has few options as stated by Broekhuizen (2016). In addition, CFD Flow Design is interoperable with other auto desk software such as revit, 3ds max and autocad architecture. The findings of Broekhuizen (2016) and the researcher's observations support the use of CFD Flow Design as a tool in determining critical wind velocity and critical wind pressure.

Conclusion

Topography in terms of elevation showed that the recorded wind pressure of the elevated houses are higher than those situated on the non-elevated areas. The turbulence of the airflow reduced when it passes through a boundary (wall, roof, tree and the like). The mathematical model as input to Computational Fluid Dynamics (CFD) Flow Design was based on the Reynolds Averaged Navier-Stokes (RANS) and Large Eddy Simulation (LES) for the turbulence model and the low Mach number assumption to decompose the pressure. Since gable roofs are light weight and flexible, they are liable to wind load and thus require a complete structural analysis and design on dead, live and wind loads.

High wind speeds, which are not yet included in the National Structural Code of the Philippines (NSCP), were used to investigate the effect of these wind velocities on the sample subdivision. As the velocity profile and elevation of the topography increases, the simulated pressure also increases. The simulated pressures at different velocities have values which are comparable to the theoretical pressure based on the Duchemin's formula. The simulated pressure results are higher than the minimum/reference theoretical pressure in which higher values indicate a more conservative/safe structural design. The higher the simulation resolution, the more detailed and accurate are the results.

Recommendation

Based on the results of this study, the following are recommended: that the wind pressure data can be used by a structural engineer as input data in designing building structures located at Cabantian, Davao City; that the wind pressure data obtained from the simulation shall be compared against the wind pressure equation of the National Structural Code of the Philippines (NSCP) 2015 for further validation of the results; that the Computational Fluid Dynamics (CFD) Flow Design may be used to analyze external wind pressures around high rise buildings and any other type of land topography for future studies as cited by Lee et al (2009) and Irshad (2012) but must take into account the wind speed factor to consider the logarithmic wind profile effect as the elevation from a reference point (at sea level) goes higher and higher.

REFERENCES

Ahmad, S., Muzzammil, M. and Zaheer, I. 2011. Numerical prediction of wind loads on low buildings. Retrieved from https://www.ajol.info/index.php/ijest/article/view/68567

Araujo, A. M., de Alencar Valenca, D. A., Asibor, A. I. and Rosas, P. A. C. (2012). An approach to simulate wind fields around an urban environment for wind energy application. Retrieved from https://link.springer.com/article/10.1007/s10652-012-9258-z

Assaad, B. 2015. Wind effect on super-tall buildings using computational fluid dynamics and structural dynamics. Retrieved from https://fau.digital.flvc.org/islandora/object/fau%3A31260/datastream/OBJ/view/Wind_effect_on_super-tall_buildings_using_computational_fluid_dynamics_and_structural_dynamics.pdf

Autodeskcfd. 2016. Fluid Flow Definitions. Retrieved from https://knowledge.autodesk.com/support/cfd/learn-explore/caas/CloudHelp/cloudhelp/2017/ENU/SimCFD-Learning/files/GUID-4DAF0D6D-F1F4-4E90-A9C8-5CACB85E79BE-htm.html

Autodeskcfd-fd. 2015. Simulation. Retrieved from https://knowledge.autodesk.com/support/flow-design/learn-explore/caas/CloudHelp/cloudhelp/ENU/FlowDesign/files/GUID-290D85CF-7A15-463C-A924-4423AEDF6B7F-htm.html

Bhandari, N. M., Krishna, P. and Kumar, K. 2011. An explanatory handbook on proposed IS 875 (part3) wind loads on buildings and structures. Retrieved from http://www.iitk.ac.in/nicee/IITK-GSDMA/W06.pdf

Boudreau, H. S. (2009). Design, construction and testing of an open atmospheric boundary layer wind tunnel. Retrieved from http://www.docdatabase.net/more-169-2009-harold-sherwood-boudreau-iii-david-o-prevatt-1160222.html

Broekhuizen, I. 2016. Integrating outdoor wind simulation in urban design: A comparative study of simulation tools and their benefits for the design of the LTU campus in Lulea. Retrieved from http://www.diva-portal.org/smash/ get/diva2: 1028220/ FULLTEXT02

Clannachan, G. H., Lim, J. B. P., Bicanic, N., Taylor, I. and Scanlon, T. J. 2009. Practical application of CFD for wind loading on tall buildings. Retrieved from http://strathprints.strath.ac.uk/13641/1/Scanlon_TJ_%26_Taylor_IJ_-_strathprints_-_Practical_application_of_CFD_for_wind_loading_on_tall_buildings_18_Nov_09.pdf

Cui, B. 2007. Wind effects on monosloped and sawtooth roofs. Retrieved from http://tigerprints.clemson.edu/ cgi/viewcontent. cgi?article=1091 and context=all_dissertations

Dagnew, A. K. and Bitsuamlak, G. T. 2012. Computational evaluation of wind loads on buildings: a review. Retrieved from https://www.researchgate.net/profile/G_Bitsuamlak/publication/264178024_Computational_evaluation_of_wind_loads_on_buildings_A_review/links/55a5fcdc08ae5e82ab1fcdee/Computational-evaluation-of-wind-loads-on-buildings-A-review.pdf

Endalew, A. M., Hertog, M., Delele, M. A., Baetens, K., Persoons, T., Baelmans, M., Ramon, H., Nicolai, B. M. and Verboven, P. 2009. CFD modeling and wind tunnel validation of airflow through plant canopies using 3D canopy architecture. Retrieved from http://www.sciencedirect.com/science/article/pii/S0142727X08001793

Gallant, L. 2014. Wind load simulation in autodesk robot structural analysis professional. Retrieved from http://bimandbeam.typepad.com/files/wind-load-simulation-in-autodesk-robot-structural-analysis-professional.pdf

Hang, J., Sandberg, M. and Li, Y. 2009. Effect of urban morphology on wind condition in idealized city models. Retrieved from https://www.researchgate.net/publication/248344075_Effect_of_urban_morphology_on_wind_condition_in_idealized_city_models

Holmes, J. D. 1986. Wind Pressures on Tropical Building Low-Rise Building. J. Wind Eng. Industr. Aerodyn., 1986, 53, No. 1-2, pp. 105–123.

Holmes, J. D. 1994. Wind pressures on tropical housing. Retrieved from http://www.sciencedirect.com/science/ article/pii/0167610594900213?via%3Dihub

Irshad, W. 2012. Wind resource assessment: statistical and computational fluid-dynamic analysis. Retrieved from https://www.napier.ac.uk/~/media/worktribe/output-191858/00thesisfinaldraftpdf.ashx

Jing, X. and Li, Y. 2013. Wind tunnel test for wind pressure distribution on gable roof buildings. Retrieved from https://www.hindawi.com/journals/tswj/2013/396936/

Kanda, M. and Maruta, E. 1993. Characteristics of fluctuating wind pressure on long low-rise buildings with gable roofs. Retrieved from https://www.researchgate.net /publication/238168100_ Characteristics_ of_fluctuating_wind_ pressure_ on_ long_low-rise_buildings_with_gable_roofs

Kerklaan, R. A. G. 2006. Design tools for the virtual wind tunnel: setting up the geometry for CFD calculations. Retrieved from https://repository.tudelft.nl/islandora/object/uuid:b81191e8-d955-4942-9dda-fe36348161e1?collection=education

Labovsky, J. and Jelemensky, L. 2013. CFD-based atmospheric dispersion modeling in real urban environments. Retrieved from https://link.springer.com/article/10.2478/s11696-013-0388-7

Lee, S. J., Park, C. W. and Kang, J. H. 2009. Evaluation of wind environment around a residential complex using a PIV velocity field measurement technique. Retrieved from https://link.springer.com/article/10.1007/s10652-009-9133-8

Meecham, D., Surry, D. and Davenport, A. G. 1991. The Magnitude and Distribution of Wind-Induced Pressures on Hip and Gabled Roofs. Retrieved from http://www.sciencedirect.com/science/article/pii/016761059190046Y?via%3Dihub

Mohotti, D., Mendis, P. and Ngo, T. 2014. Application of computational fluid dynamics (cfd) in predicting the wind loads on tall buildings - a case study. Retrieved from http://epubs.scu.edu.au/cgi/viewcontent.cgi?article=1168 and context=acmsm23

Montazeri, H. and Blocken, B. 2013. CFD simulation of wind-induced pressure coefficients on buildings with and without balconies: validation and sensitivity analysis. Retrieved from http://citeseerx.ist.psu.edu/viewdoc /download?doi= 10.1.1.709. 3739 and rep=rep1 and type=pdf

Moukalled, F., Darwish, M. and Mangani, L. 2016. The Finite Volume Method in Computational Fluid Dynamics: An Advanced Introduction with Open FOAM and Mathlab. Retrieved from http://www.gidropraktikum.narod.ru/Moukalled-et-al-FVM-OpenFOAM-Matlab.pdf

Murakami, S., Ooka, R., Mochida, A., Yoshida, S. and Kim, S. 1999. CFD analysis of wind climate from human scale to urban scale. Retrieved from http://www.sciencedirect.com/science/article/pii/S0167610599000094

National Disaster Risk Reduction and Management Council. (2014). Effects of Typhoon Haiyan (Yolanda). Retrieved from http://ndrrmc.gov.ph/attachments/article/1329/Update_on_Effects_Typhoon_YOLANDA_(Haiyan)_17APR2014.pdf

Patankar, S. V. and Spalding, D. B. 1972. A calculation procedure for heat, mass and momentum transfer in three-dimensional parabolic flows. Int. J. of Heat and Mass Transfer, Volume 15, Issue 10, October 1972, Pages 1787-1806.

Prasad, D., Uliate, T. and Ahmed, M. R. 2008. Wind loads on low-rise building models with different roof configurations. Retrieved from https://www.researchgate.net/publication/235337291_Wind_Loads_on_Low-Rise_Building_Models_with_Different_Roof_Configurations

Reiter, S. 2008. Validation process for CFD simulations of wind around buildings. Retrievedfrom https://orbi.ulg.ac.be/ bitstream/ 2268/204 00/1/EBE-Reiter.pdf

Robinson, S. 2004. Simulation: The Practice of Model Development and Use. Retrieved   from   https://he.palgrave.com/ resources/ sample- chapters/ 9781137328021_sample.pdf

Wakes, S. J., Maegli, T., Dickinson, K. J. and Hilton, M. J. 2009. Numerical modeling of   wind   flow   over   a   complex topography. Retrieved from http://www.sciencedirect.com/science/article/pii/S136481520900200X

****